

UCLA

UCLA Previously Published Works

Title

How auditory neurons count temporal intervals and decode information

Permalink

<https://escholarship.org/uc/item/57p0p1tt>

Journal

Proceedings of the National Academy of Sciences of the United States of America,
121(35)

ISSN

0027-8424

Authors

Alluri, Rishi K

Rose, Gary J

McDowell, Jamie

et al.

Publication Date

2024-08-27


DOI

10.1073/pnas.2404157121

Peer reviewed



How auditory neurons count temporal intervals and decode information

Rishi K. Alluri^{a,1} , Gary J. Rose^a, Jamie McDowell^b , Anwesh Mukhopadhyay^a , Christopher J. Leary^c, Jalina A. Graham^d, and Gustavo A. Vasquez-Opazo^e

Affiliations are included on p. 11.

Edited by Earl Miller, Massachusetts Institute of Technology, Cambridge, MA; received February 27, 2024; accepted July 5, 2024 by Editorial Board Member Peter L. Strick

The numerical sense of animals includes identifying the numerosity of a sequence of events that occur with specific intervals, e.g., notes in a call or bar of music. Across nervous systems, the temporal patterning of spikes can code these events, but how this information is decoded (counted) remains elusive. In the anuran auditory system, temporal information of this type is decoded in the midbrain, where “interval-counting” neurons spike only after at least a threshold number of sound pulses have occurred with specific timing. We show that this decoding process, i.e., interval counting, arises from integrating phasic, onset-type and offset inhibition with excitation that augments across successive intervals, possibly due to a progressive decrease in “shunting” effects of inhibition. Because these physiological properties are ubiquitous within and across central nervous systems, interval counting may be a general mechanism for decoding diverse information coded/encoded in temporal patterns of spikes, including “bursts,” and estimating elapsed time.

Counting | numerical abilities | time perception | burst decoding | neural mechanisms

Animals across taxa, ranging from insects to primates, possess numerical abilities (1–4). In contrast to the familiar “label-based,” i.e., symbolic, counting process employed by humans, many animal species possess innate, nonsymbolic mechanisms for assessing the numerical value (“numerosity”) of a set of objects. While short-term, abstract pattern recognition processes may underlie some forms of spatial numerosity, identifying the number of scanned objects or events that occur sequentially with a particular timing, e.g., acoustic elements, must involve memory and tallying of past events (5, 6). This interval-specific numerical ability is critical for the acoustic communication of many animals and may represent a phylogenetic precursor for the musical sense of humans. Although numerical abilities have been extensively studied, the mechanisms that underlie “innate counting” processes and, therefore, the “number sense” of animals are incompletely understood.

Neurons that respond most strongly for values of spatial numerosity, i.e., the number of objects in a scene, have been identified in telencephalic regions of human (7) and nonhuman (8, 9) primates and birds (10, 11). Neural substrates of interval-specific numerical abilities, however, are less well characterized. Neurons have been recorded in the anuran inferior colliculus (IC_{an}) that respond only after at least a threshold number of precisely timed sound pulses (notes) have occurred (12–16) (Fig. 1 *A* and *B*). Pulse-number thresholds (PNTs) result from a counting process, not simply stimulus energy (12, 17); correspondingly, a single aberrantly long interval between successive pulses can completely reset the counting process (12, 13). These “interval-counting neurons” (ICNs) selectively count the number of pulses that have biologically relevant intervals (18); in northern leopard frogs, ICNs are selective for pulse rates largely in the 30 to 90 pulses/s range, as found in natural vocalizations such as “grunts” and “chuckle” calls. ICNs, therefore, constitute temporal selectivity filters and counters. In vision, this process may bear similarity to counting the number of objects of a particular shape in a complex scene that comprises many different types of objects.

More generally, ICNs could be important for decoding information represented in temporal patterns of spiking. For example, sequences of precisely timed spikes, i.e., “bursts,” have been postulated to encode salient information, including memories (19, 20). Information may even be encoded in the number of spikes in a burst that occur with particular timing (21). ICNs could decode information in these bursts and provide a temporal-to-“place” (site of activity) transformation of encoding (Fig. 1 *C*). Further, ICNs could be used to estimate elapsed time. Interval counting is an essential, but poorly understood, component of

Significance

Numerical abilities are widespread across taxa, but the underlying neural basis is poorly understood. The anuran auditory system, which has neurons that count temporal intervals, is particularly well suited for investigating the numerosity sense. Here, we combined whole-cell recordings, *in vivo*, with focal pharmacological manipulations and estimation of excitatory and inhibitory conductances to show that counting is achieved when excitation, augmented over successive pulses, occurs within the temporal interval between the onset and offset phases of inhibition. Further, nonlinear shunting inhibition shaped the amplitude and selectivity of excitation, thereby contributing to interval counting. This work advances our mechanistic understanding of counting and sheds light on the origins of interval-based numerical abilities in animals.

The authors declare no competing interest.

This article is a PNAS Direct Submission. E.K.M. is a Guest Editor invited by the Editorial Board.

Copyright © 2024 the Author(s). Published by PNAS. This article is distributed under [Creative Commons Attribution-NonCommercial-NoDerivatives License 4.0 \(CC BY-NC-ND\)](https://creativecommons.org/licenses/by-nc-nd/4.0/).

¹To whom correspondence may be addressed. Email: rishi.alluri@utah.edu.

This article contains supporting information online at <https://www.pnas.org/lookup/suppl/doi:10.1073/pnas.2404157121/-DCSupplemental>.

Published August 19, 2024.

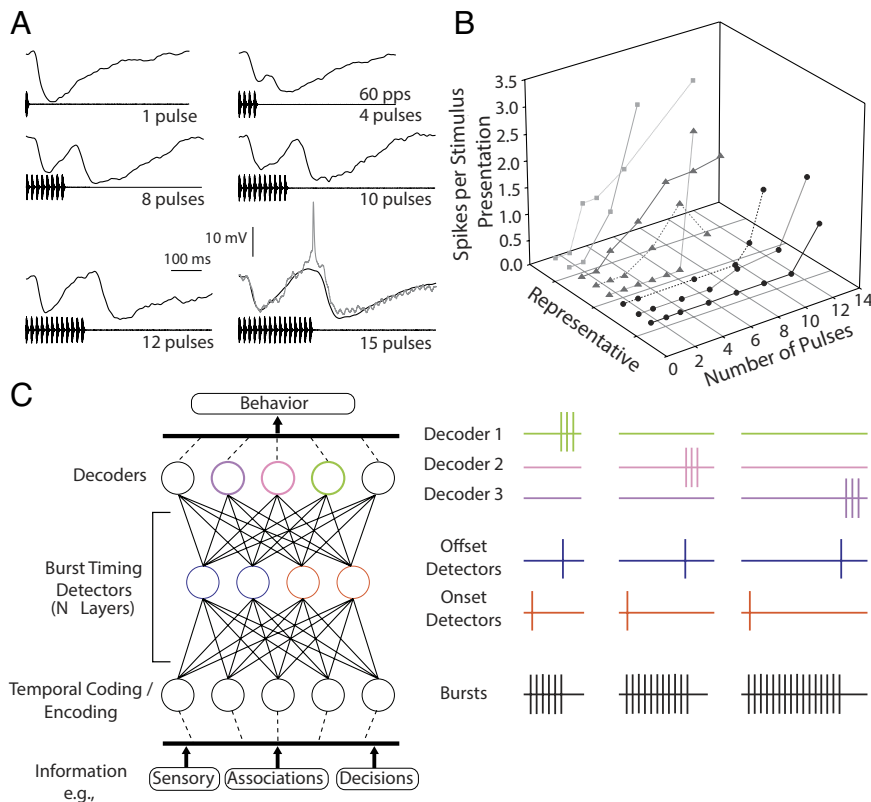


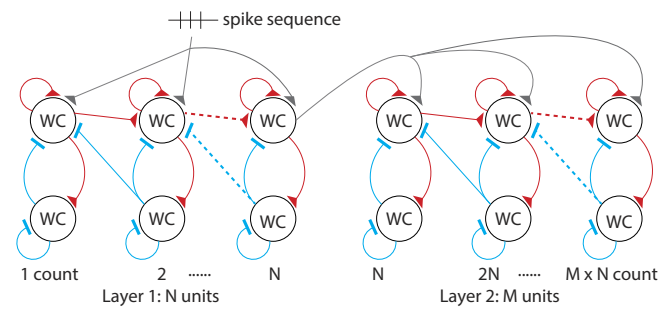
Fig. 1. Electrophysiological characteristics of interval-counting neurons (ICNs), burst decoding, and mechanistic models. (A). Whole-cell membrane potential recordings from an ICN with pulse-number threshold of 14; shown are single (gray traces) and averaged (black traces) responses to stimuli in which pulse rate was held at 60 pulses/s and pulse number was varied. Spikes were removed for averaging. (B) 3-d line plots of the number of spikes per stimulus presentation (SPS) vs the number of pulses in the stimulus, for 8 cells in the anuran (*R. pipiens*) inferior colliculus that represent the observed range of pulse number selectivity. Neurons that required 2 to 3 (light gray), 4 to 7 (medium gray), or 8 to 12 (black) pulses to reach threshold response levels are shown. (C) Schematic depicting coding or encoding information in the temporal discharge patterns (“bursts”) of central neurons, which ICNs then decode to create a “place code” of information.

“pacemaker-accumulator” models for estimating the time that has elapsed from some starting event. In these models, unspecified neuronal processes count pacemaker pulses and compare them to stored reference values. Recently, Zemlianova et al. (22) have constructed a neuronal instantiation of this model that can count events and estimate elapsed time (Fig. 2A). This model uses feedforward excitation to encode the number of events in the position of activity within a spatial network.

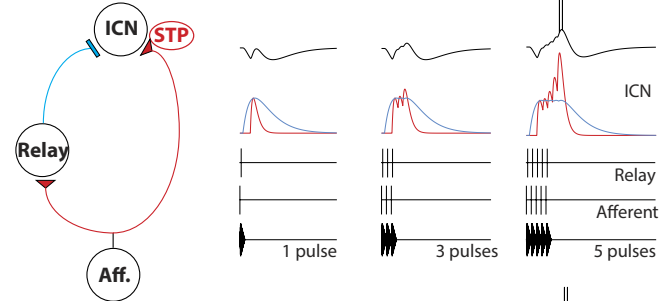
As these examples illustrate, it is of considerable interest and importance to understand the computational mechanisms that underlie interval counting. An important question is whether interval counting is mechanistically rooted in basic circuit properties that are present across a wide range of brain structures and nervous systems. While some progress has been made, the mechanisms that underlie interval counting have remained elusive. Initial whole-cell patch recordings from ICNs, in vivo, revealed an interplay between excitation and inhibition (13). The long time course of inhibitory postsynaptic potentials (IPSPs) to individual pulses (Fig. 1A), along with persistent hyperpolarization following a series of pulses, suggested that rate-dependent augmentation of excitation was required to overcome this inhibition (Fig. 2B). From modeling experiments, however, Naud et al. (23) postulated that a more complex constellation of activity-dependent plasticity, including rate-dependent depression of inhibition (“dis-inhibition”) and offset inhibition (Fig. 2C), is required to effectively generate temporal patterns of hyperpolarization and depolarization that matched those observed in some whole-cell patch recordings. In the independent Zemlianova et al. model of counting (22), a processing unit switches to a high activity state when the excitation

from a preceding unit sums with the input excitation from a pacemaker or the output of the previous layer. Although, as in other models, inhibition is present and ensures that the representational activity is sparse, it is not required for counting; nevertheless, the feedforward excitation structure could contribute to the interval-counting properties of ICNs. To further evaluate these models and elucidate the mechanisms that underlie this counting process, we took advantage of recent advances in combining whole-cell patch recordings with focal pharmacology, in vivo, and conductance reconstructions (24); this methodological approach has provided deep insights into mechanisms of neural processing (25, 26). We utilized the anuran auditory system, which provides the opportunity to perform these experiments in mechanically stable (attributable to cutaneous respiration), unanesthetized animals. We made whole-cell patch recordings from ICNs at several levels of negative current “clamp” (SI Appendix, Fig. S1) and then mathematically estimated (Methods, Eqs. 1–4) the time courses of excitatory and inhibitory conductances across a range of pulse numbers. We also attenuated inhibition pharmacologically to directly assess its role in interval counting. Results of these experiments reveal that interval counting in most cases arises from integrating phasic, onset-type and offset inhibition with excitation that is augmented with successive intervals—potentially because of a progressive decrease in “shunting” effects of inhibition. Because these physiological properties are ubiquitous within and across central nervous systems, this interval counting mechanism could potentially underlie interval-specific numerosity, decoding information encoded in spike bursts and neuronal estimation of elapsed time.

A Zemlianova et al., 2022



B Edwards et al., 2007



C Naud et al., 2015

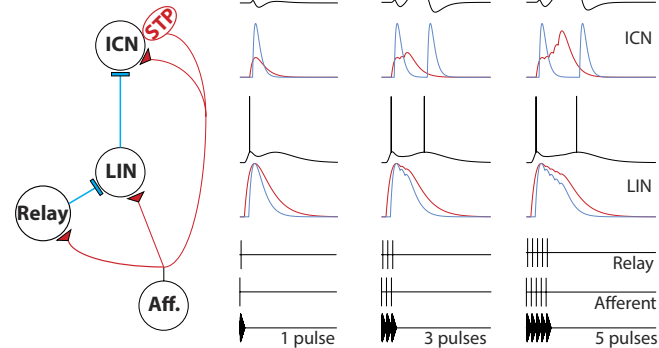


Fig. 2. Models of interval counting. (A) A sequentially activated hierarchical-place model (Zemlianova et al., 2022) that reads temporal patterns of input spikes. Each layer consists of circularly connected Wilson-Cowan (WC) units; each unit supplies feedforward excitation and, in turn, receives feedback inhibition. Successive layers count in multiples of the preceding layer's output count. (B) Rate-dependent augmentation of excitation (Edwards et al., 2007) and (C) dis-inhibition (Naud et al., 2015) models for generating interval selectivity and counting. Neurons that show selectivity for long intervals (LINs) provide inhibition (blue projections) to ICNs; some excitatory inputs (red) show augmenting-type short-term plasticity (STP).

Results

ICNs respond only after a threshold number of sound pulses have occurred with cell-specific intervals. To investigate the mechanisms that underlie this counting process, we made recordings from 63 ICNs (49 whole-cell and 14 extracellular recordings), in vivo, in the anuran inferior colliculus (IC_{an}); PNTs (eliciting spikes on $\geq 50\%$ of stimulus presentations) ranged from 2 to 14 (median = 5), e.g., Fig. 1B. We were able to record sufficient data to estimate stimulus-elicited excitatory (Δg_e) and inhibitory (Δg_i) conductances for 27 of these cells. We first show representative recordings and estimates of excitatory and inhibitory conductances for neurons that mostly span this range of PNTs.

Recordings and conductance traces for a neuron that had a PNT of 2 are shown in Fig. 3A; that is, this cell spiked in response to stimuli that had 2 or more pulses, broadcast with interonset intervals

of 16.67 ms. This neuron, which represented 3 others in this study, showed short-latency (~ 20 ms) excitation and delayed inhibition; this onset disparity resulted in early, relatively transient, net excitation (filled, red region; $(\Delta g_e - \Delta g_i) > 0$) that was suprathreshold for stimuli with more than 1 pulse. Excitation and inhibition increased in amplitude and duration with increasing pulse number; as a result, the net excitation (net Δg_e) was substantially less than the gross excitation (mean Δg_e) (filled vs striped, red histogram bars), indicating that, across stimuli, inhibition counteracted all but the early phase of excitation. Inhibition appeared to limit the duration of stimulus-elicited depolarizations in this and the 3 other cases that had PNTs of 2 to 3.

Fig. 3B shows recordings and conductance estimates for a cell that had a PNT of 5 to 6 pulses, presented at 30 pulses/s (pps). In this and 4 other cases, e.g., *SI Appendix*, Fig. S1, the pulse periodicity was reflected in a corresponding periodicity of conductance fluctuations. In contrast to neurons with PNTs of 2 to 3, the onsets of inhibition and excitation in this cell were more coincident. Importantly, the inhibitory conductance had both early (onset) and late (offset) components, which were particularly evident for stimuli that had 4 or more pulses; the onset inhibition depressed in amplitude, resulting in a clear temporal separation between these phases of inhibition. In this temporal “window”, inhibition minimally opposed excitation. The net Δg_e (red, filled traces and histogram bars), therefore, increased nonlinearly, relative to the mean Δg_e , as pulse number was increased from 1 to 6. Spike responses more closely followed the net excitation. In contrast, there was comparatively little change in net Δg_i over this range in pulse number, likely because stimuli having few pulses elicited both onset and offset inhibition; note that the duration of Δg_i for 2 pulses was substantially greater than that of the onset phase of inhibition at PNT. For the case shown in Fig. 3C, full separation between onset and late phases of inhibition, i.e., onset inhibition reached its fully depressed level, occurred at ~ 10 pulses, presented at 90 pulses/s. For the 10-pulse stimulus, the late phase of the inhibition began ~ 13 ms before the end of the stimulus, possibly resulting from rebound of the onset inhibition; this property was observed in 5 other cases. Between 8 and 10 pulses, the transition to spiking, mean (gross) and net Δg_e increased 77% and 82%, respectively. In contrast, in changing pulse number from 5 to 8, mean and net Δg_e increased 169% and 771%, respectively. This nonlinear increase in net excitation from 5 to 8 pulses corresponded with the separation of onset and late phases of inhibition and contributed, along with the large increase in mean Δg_e , to the high PNT of this neuron. Because excitation increased nonlinearly over this range in pulse number, net Δg_e increased less than mean Δg_e . Similar dynamics of inhibition and nonlinear increases in net excitation with pulse number are evident in the case shown in *SI Appendix*, Fig. S1, which had a PNT of 7 to 8; this case, however, showed a particularly strong nonlinearity in mean Δg_e with pulse rate. From 2 to 8 pulses, net Δg_e increased only $\sim 50\%$, whereas net Δg_e increased ~ 20 fold. Thus, for these ICNs, inhibition was strong and differentially opposed excitation across pulse numbers; inhibition counteracted excitation to stimuli with few pulses but, near PNTs, excitation largely fell in the temporal window between onset and offset inhibition. Net Δg_e , therefore, continued to increase with pulse number. The increase in net Δg_e with pulse number was largely due to the unopposed late/offset inhibition, which we will next show is important for resetting the interval counting process.

Lengthening a Single Interval Reinstates Inhibition and Resets Counting. Onset-type inhibition appears to depress with pulses repeated at sufficiently fast rates and additional inhibition occurs

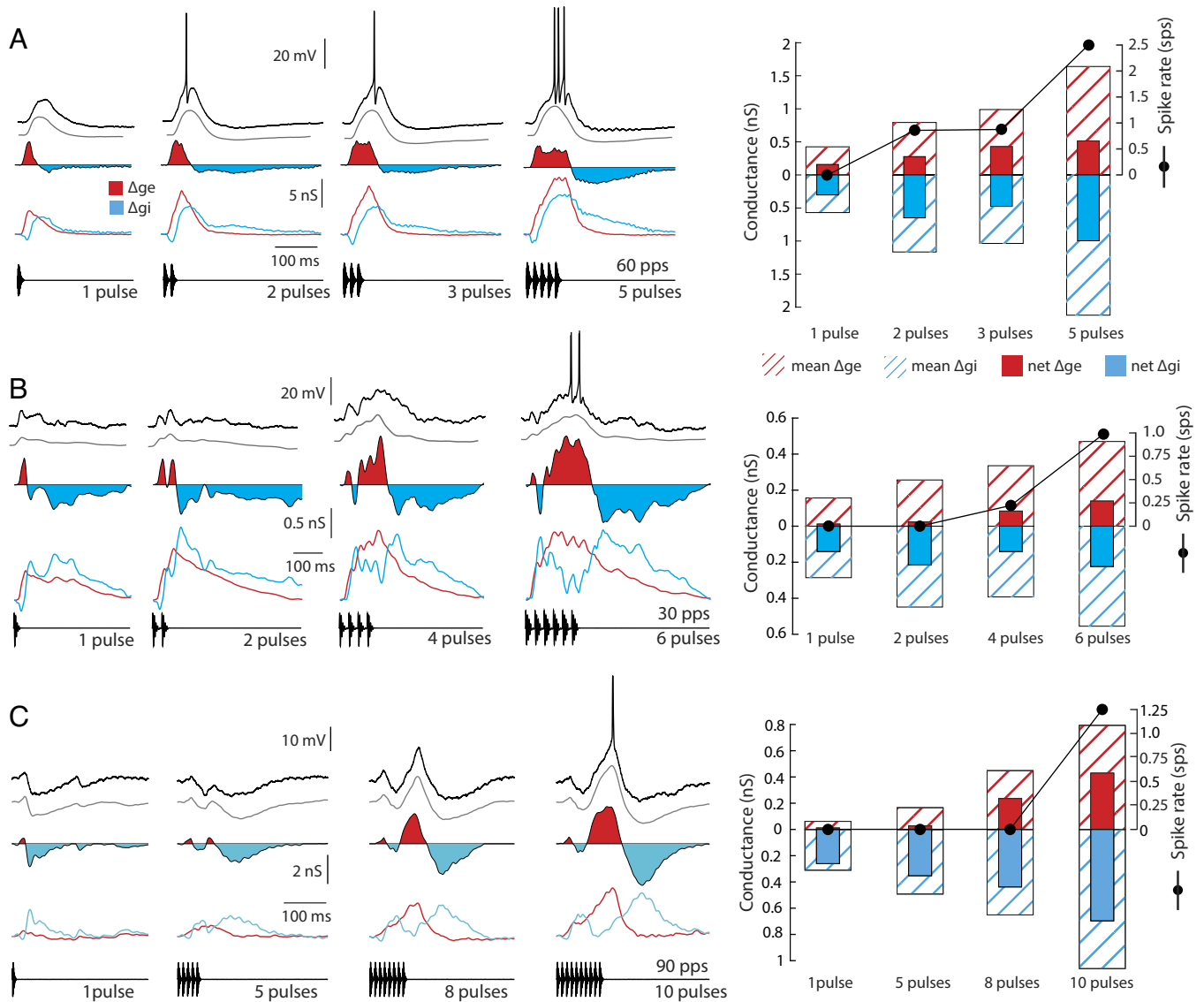


Fig. 3. Patterns of excitation and inhibition to ICNs across their interval-counting range: The importance of dis-inhibition. Whole-cell membrane potential recordings and estimates of excitatory (Δg_e , red) and inhibitory (Δg_i , blue) conductances, along with area plots of their difference, for interval-counting neurons (ICNs) with PNTs of 2 (A), 5 (B), and 10 (C) pulses; stimulus pulse rates were 60, 30, and 90 pulses/s, respectively. Recordings show single (black traces) and averaged (gray traces) responses to stimuli with pulse numbers shown; spikes were removed for averaging. Slight decreases in Δg_i below baseline are artifactual (see *Methods*). Bar plots (Right) show mean excitatory (Δg_e , red striped) and inhibitory (Δg_i , blue striped) conductances, net Δg_e (filled red, see *Methods*) and net Δg_i (filled blue), and spike rate measured as spikes per stimulus presentation (SPS; black line with solid circles) in response to stimuli with pulse numbers shown. (A)–(C): Resting potentials = -68 , -82 , and -51 mV; carrier frequencies = 1,600, 210, and 700 Hz; stimulus amplitudes = 67, 78, and 76 dB SPL, respectively.

following stimulus offset. Lengthening a single interval in a series of pulses might, therefore, elicit additional inhibition and, thereby, reset the interval-counting process (12). To investigate the mechanistic basis of this resetting phenomenon, in 3 cases we calculated excitatory and inhibitory conductance responses to pulse sequences in which the middle interval (interpulse onset) was progressively increased. An exemplar, shown in Fig. 4, had a PNT of 13 to 14 pulses, and responded strongly to a series of 25 pulses presented at 70 pulses/s. Consistent with the results shown in Fig. 3, this ICN showed onset and offset inhibition. The onset inhibition depressed to baseline level within ~ 170 ms after stimulus onset, enabling the tonic excitation to elicit suprathreshold depolarization and ~ 2.9 spikes per stimulus presentation. Offset inhibition at the end of the pulse sequence then counteracted the excitation and hyperpolarized the cell. Increasing the interval between onsets of the 12th and 13th pulses to 20 ms (from ~ 14.3 ms) resulted in a small increase in the inhibitory conductance above its baseline level. The amplitude of this “gap inhibition”

increased and the excitation decayed as this middle interval was progressively lengthened and, at 50 ms, reached the level of the onset inhibition. For this 50 ms condition, the pulse sequences that preceded (12 pulses) and followed (13 pulses) the long interval rarely elicited spikes and at approximately the same level (1 spike in 9 presentations of the stimulus), indicating that the interval-counting process had been reset. Across cases, the inhibition that occurred during these gaps appeared, therefore, to counteract excitation, evident as a progressive decrease in net Δg_e (filled, red bars in histogram) as the duration of the gap was increased; this process resulted in a repolarization of the membrane and reset the interval-counting process. The decay in excitatory conductance during the longer intervals was also observed in a case that showed little or no inhibition (*SI Appendix, Fig. S2*). Unexpectedly, the overall mean Δg_e also decreased as the duration of the middle interval was increased; this apparently anomalous result may be related to shunting effects of inhibition, which was elucidated only after pharmacologically attenuating inhibition (see below).

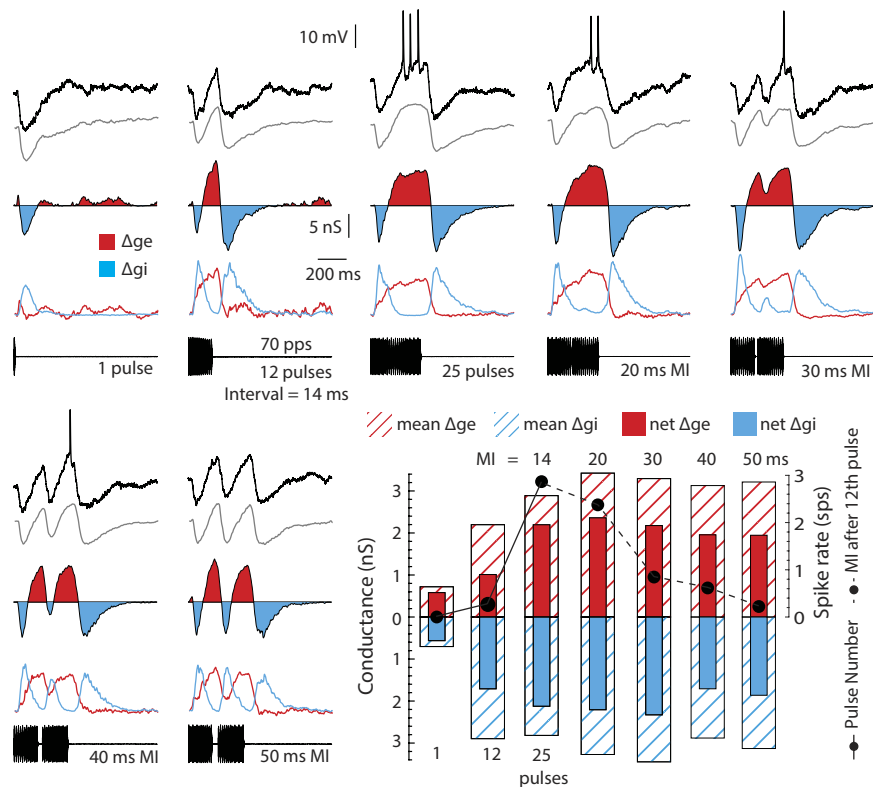


Fig. 4. A single long interval reinstates inhibition and can reset the interval-counting process. Whole-cell membrane potential recordings and estimates of excitatory (Δg_e , red) and inhibitory (Δg_i , blue) conductances, along with area plots of their difference, for an interval-counting neuron (ICN) that required approximately 14 pulses, presented at 70 pulses/s, to spike. The interval between onsets of the 12th and 13th pulses, i.e., middle interval (MI), in a sequence of 25 pulses, was progressively increased from ~16.67 ms to 50 ms, resulting in recovery of inhibition. Responses to the pulse sequences preceding and following the gap were similar for a MI of 50 ms. Bar plots, as in Fig. 2. Resting potential = -45 mV; carrier frequency = 1,550 Hz; stimulus amplitude = 57 dB SPL.

A Temporal Window Through Inhibition and Nonlinear Increase in Excitation Contribute to Interval Counting.

Across ICNs that showed clear inhibition, PNTs were strongly related to the pulse number at which full separation of onset and late phases of inhibition occurred ($r^2 = 0.65$, $P < 0.001$, $n = 13$) (Fig. 5A); inhibition counteracted excitation most strongly for pulse numbers well below threshold. For many of these ICNs the net Δg_e , therefore, changed (% drop from PNT to 1 pulse, see Methods Eq. 5) at a greater rate than did the mean Δg_e (Fig. 5B), i.e., data points fell below the 1:1 line (drop in mean Δg_e = drop in net Δg_e)—particularly over the range in pulse number for which onset and offset inhibition dissociated. Cases that appeared to have little, if any, inhibition (open circles) fell along the 1:1 line. Across all cells, the amplitude of mean Δg_e to single pulses, relative to that at PNT (Fig. 5C, Eq. 6), was negatively related to PNTs ($r^2 = 0.39$, $P < 0.001$, $n = 26$); that is, ICNs tended to have higher PNTs if excitation to single pulses was weak. Nevertheless, ICNs for which excitation to single pulses was weak varied considerably in PNTs (Fig. 5C). As shown in Fig. 5A, the pulse number at which onset and offset components of inhibition separated accounted for much of this variation. Nonlinear increases of excitation with pulse number also played a critical role in determining PNTs (Fig. 5D), even for some ICNs that exhibited prominent inhibition, e.g., Fig. 3C, S1; in these cases, the drop in mean and net excitation were similar (fall along the 1:1 line). The pulse number at which the change in mean Δg_e (slope, Eq. 7, Methods) was greatest, i.e., largest change in mean Δg_e per unit increase in pulse number, strongly predicted PNTs ($r^2 = 0.63$, $P < 0.001$, $n = 26$). Adding to the model the normalized Δg_e to 1 pulse accounted for only an additional ~6% of the variation in PNTs ($r^2_{\text{adj}} = 0.69$, $P < 0.001$, $n = 26$).

Cells that showed prominent inhibition and weak excitation that increased nonlinearly only after many pulses had occurred, e.g., Fig. 3C and SI Appendix Fig. S1, tended to have high PNTs, even if temporal separation of onset and offset inhibition occurred at lower pulse numbers (e.g., light-green square, Fig. 5A); that is, the opening of a window between onset and offset inhibition was necessary, but not always sufficient for achieving a threshold response. The temporal “window” through the inhibition was critical, however, for ICNs that had mid- to high PNTs and strong excitation that increased rather linearly with pulse number, e.g., Fig. 3B. Notably, the temporal window in the inhibition largely determined the PNTs of ICNs that showed maximal increase in excitation at 2 pulses and accounted for the substantial variation in their PNTs (Fig. 5D). The outlier point (PNT=10 pulses, maximum slope of mean Δg_e at 2 pulses) in Fig. 5D was an ICN that showed little or no inhibition and spikes were elicited only at the asymptote of excitation, i.e., excitation was marginally sufficient for triggering spikes (SI Appendix, Fig. S2).

Nonlinear increases in excitation with pulse number, were critical in determining the interval-counting properties of ICNs that showed little or no inhibition (fell along the 1:1 line in Fig. 5B), as is evident in the representative case shown in Fig. 6. The mean excitation (Δg_e) to this cell was subthreshold, i.e., no spikes were elicited, for stimuli with fewer than approximately 6 to 7 pulses and increased 135% and 150% for responses to 4 vs 6 pulses and 6 vs 8 pulses, respectively. The PNT for this neuron was 9 pulses.

To further investigate the role of excitation in determining PNTs, we iontophoresed NBQX (antagonist of AMPA-type glutamate receptors) to pharmacologically attenuate excitation ($n = 3$). Increases in excitation with pulse number might be important for determining PNTs; that is, excitation at PNT may be only slightly

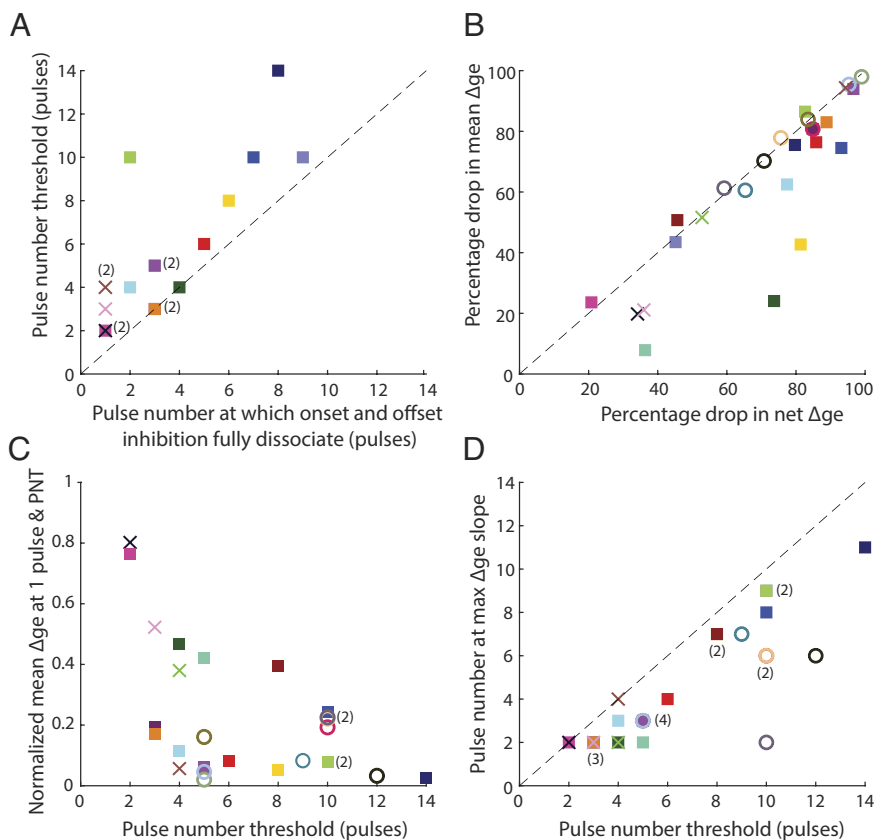


Fig. 5. Full separation of onset and late-phase inhibition is computationally significant in determining pulse number thresholds. (A) Relationship between pulse- (interval) number threshold and pulse number at which full temporal separation of onset and late-phase (offset) inhibition occurred (square symbols). Crosses indicate pulse-number thresholds of cells that showed delayed-onset, but not offset, inhibition. (B) Drop of the mean vs. drop in net excitatory conductance from pulse-number threshold to 1 pulse. Cells are characterized by whether inhibition was apparent (squares & crosses) or not (open circles). In all plots, the dashed line indicates a 1:1 relationship. (C) Amplitude of mean excitatory conductance to 1 pulse relative to that at pulse-number threshold (PNT) vs. PNT for 26 interval-counting neurons. (D) Pulse number at which the change of mean excitatory conductance (Δg_e) per pulse was maximal vs. PNT.

suprathreshold. In this case, PNT should increase appreciably if excitation is attenuated. Alternatively, however, excitation may be suprathreshold (without inhibition) even for pulse numbers well below threshold. In this case, PNT should not change appreciably following moderate attenuation of excitation; spiking should occur if the number of pulses exceeds that required for onset and offset phases of inhibition to separate. For the case shown in Fig. 7, single pulses elicited excitation that was only ~9% that to 5-pulse stimuli (0.02 nS vs. 0.22 nS), i.e., excitation increased nonlinearly with pulse number, and inhibition largely countered this weak excitation. Following iontophoresis of NBQX to attenuate excitation (~50% of baseline), PNT increased from approximately 4 to 8. This cell showed onset and offset inhibition that opposed excitation primarily for stimuli that had few pulses. Over all 3 cases, PNT increased by ~91% after NBQX. The large increase in pulse-number threshold following NBQX, therefore, most strongly supports the hypothesis that, at least in this and the other two cases, excitation to stimuli with near-threshold numbers of pulses does not greatly exceed that required for eliciting spikes. These results support the conclusion that interval counting, in many cases, results from excitation that increases nonlinearly with pulse number and inhibition that shows phasic onset and offset components.

Pharmacologically Attenuating Inhibition to ICNs Decreases PNTs and Increases Excitatory Conductance: The Role of “silent” Inhibition. The analyses of excitatory and inhibitory conductances, presented above, suggest that inhibition plays an important role in the interval-counting properties of most ICNs.

To directly test this hypothesis, we made whole-cell recordings and iontophoresed either antagonists of GABA_A receptors (bicuculline, $n = 2$ or gabazine, $n = 7$) extracellularly or fluoride (block chloride channels) intracellularly ($n = 5$) to attenuate inhibition. Both methods of attenuating inhibition decreased the PNTs of ICNs (Fig. 8; Wilcoxon Signed Rank Test, $P < 0.001$, $n = 14$), but to varying degrees across cases. With GABA_A antagonists, baseline negative current-clamp recordings can be made prior to blocking inhibition to the cell, which is potentially reversible. For KF, recording with negative current-clamp progressively loads the cell with fluoride, thereby limiting the duration of baseline recordings. A disadvantage of bicuculline or gabazine iontophoresis, however, is that inhibition to other neurons near the recorded cell might also be attenuated, and possibly influence local circuit properties. This issue surfaced in an earlier study, in which excitation to “long-interval neurons” was increased after gabazine was iontophoresed to attenuate inhibition (26). In the present experiments, we acquired sufficient current-clamp data before and after iontophoresing GABA_A antagonists to estimate excitatory and inhibitory conductances in 3 cases. Across these cells, mean excitation increased ~77% for responses to stimuli that had near-threshold numbers of pulses. For one ICN, PNT decreased from 3 to 4 (baseline) to 1 following gabazine iontophoresis and the mean excitation (Δg_e) increased 136% and 61% for 1-pulse and 4-pulse stimuli, respectively (*SI Appendix*, Fig. S3). In the second case, mean excitation to 6-pulse stimuli increased 45.6% following bicuculline iontophoresis and PNT decreased from 4 to 2. These large increases in mean excitation following iontophoresis of GABA_A antagonists raised the possibility that inhibition to

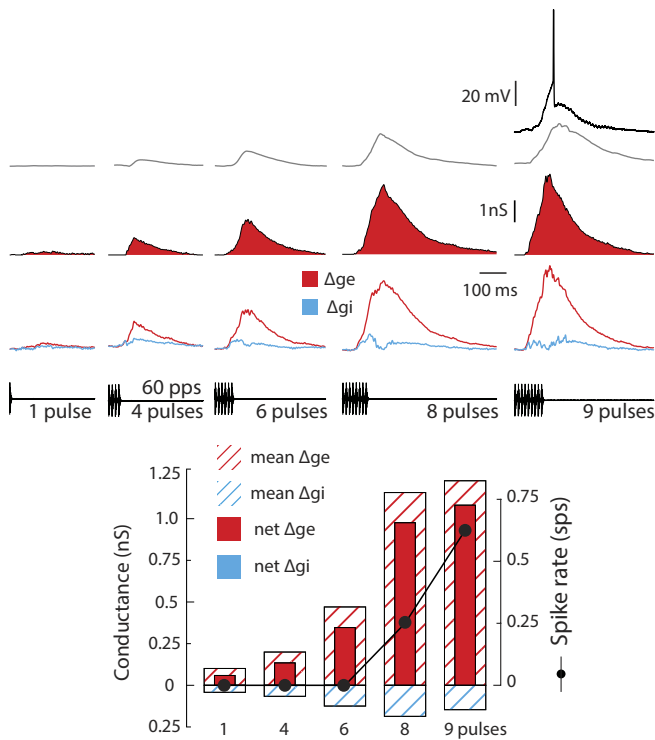


Fig. 6. Example of an interval-counting neuron that showed minimal inhibition. Whole-cell membrane potential recordings and estimates of excitatory (Δg_e , red) and inhibitory (Δg_i , blue) conductances for an interval-counting neuron (ICN) with pulse-number threshold of ~ 9 pulses, presented at 60 pulses/s. Resting potential = -82 mV; BEF = 475 Hz; stimulus amplitude = 71 dB SPL.

local-circuit excitatory afferents might have been blocked. To address whether increases in mean Δg_e occur following attenuating inhibition to only the recorded neuron, we now present results of conductance analyses for ICNs recorded with KF in the pipette.

Fig. 9 shows 2 of the 5 cases in which we made whole-cell recordings from ICNs while using KF to attenuate inhibition selectively to the recorded neuron. The neuron displayed in Fig. 9A showed prominent onset and offset inhibition, manifest as IPSPs, e.g., Fig. 3 B and C, weak excitation to 1- and 2-pulse stimuli and had a PNT of 4. The amplitude of onset IPSPs decreased from ~ 11 mV (baseline) to < 1 mV after loading the cell with Fluoride (-0.1 nA ejection current for ~ 5 min) and, with 4- or 6-pulse stimuli, the mean Δg_i decreased 78% and 77% from baseline, respectively. As was seen with GABA_A receptor antagonists, the mean Δg_e increased following KF; mean Δg_e increased $\sim 40\%$ and 94% for 1- and 2-pulse stimuli, respectively. Nevertheless, despite the augmented excitation, these stimuli still did not elicit spikes, and the PNT decreased only marginally to 3 pulses. Thus, inhibition appeared to shunt excitatory current, particularly for 1 and 2-pulse stimuli. Prior to KF, the mean Δg_e at PNT was 8-fold greater than the mean Δg_e for 1 pulse; after KF, this ratio decreased to 4. Although the mean excitation to the 4-pulse stimuli was similar before and after KF, the net excitation increased $\sim 20\%$ after KF and appeared to account for the PNT decreasing minimally from 4 to 3 pulses. In this case, therefore, inhibition opposed and appeared to shunt excitation for 1 and 2-pulse stimuli that was subthreshold.

The neuron shown in Fig. 9B had a pulse-number threshold of ~ 6 to 7 pulses and represents ICNs that appeared to have little stimulus-driven inhibition. Mean and net excitation were similar and increased proportionately from 1 to 10 pulses. Nevertheless, following loading with fluoride, the stimulus-driven mean Δg_e of this cell increased $\sim 147\%$, 31% , and 49% for 1, 5, and 10 pulse

stimuli, respectively; the disproportionately larger increase for the 1-pulse stimuli contributed to the PNT decreasing to 1 pulse. Thus, despite seeing little evidence of inhibition, fluoride markedly altered the interval-counting properties of this neuron. These results further establish that inhibition is important for determining the PNTs of ICNs and suggest that it may include a "silent" component, i.e., has a reversal potential near the resting potential, that shunts excitation to the cell.

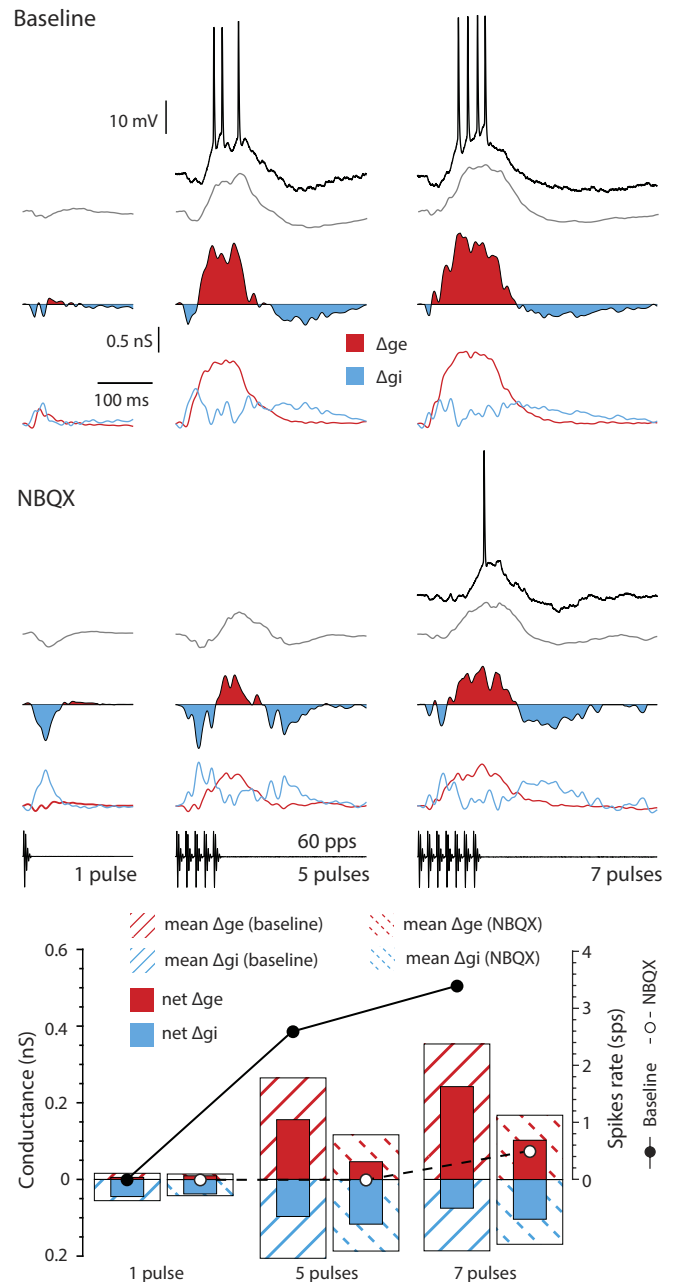


Fig. 7. Attenuating excitation increases pulse-number threshold. Whole-cell membrane potential recordings, before (upper) and after (lower) iontophoresing NBQX, an antagonist of AMPA-type glutamate receptors. Single (black) and averaged (gray) responses are shown. Estimates of changes in excitatory conductances (Δg_e , red) and inhibitory (Δg_i , blue) and their difference over time (area plots) are also shown. Mean and net conductances are displayed as striped and filled, respectively, bars in histograms; 45°- and -45°-striped bars represent baseline and NBQX conditions, respectively. Spikes per stimulus repetition are shown as solid or dotted lines for baseline and NBQX conditions, respectively. Resting potential = -54 mV; BEF = 300 Hz; stimulus amplitude = 76 dB SPL. PNTs were 4 and 8 pulses before and after NBQX, respectively.

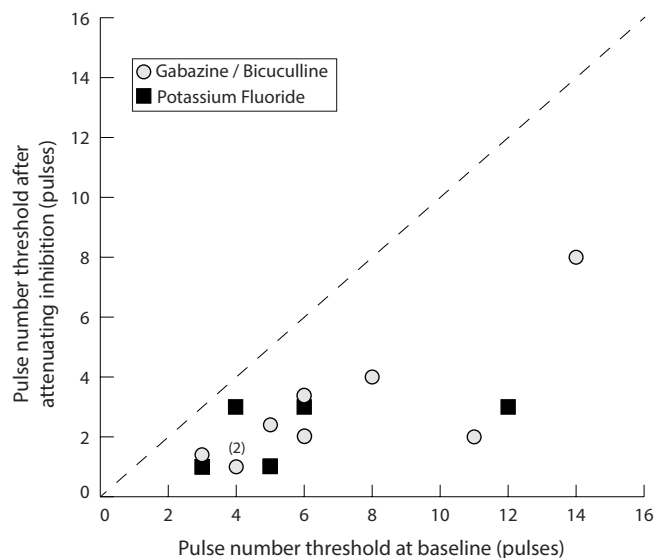


Fig. 8. Pharmacological evidence that inhibition is critical for selectivity in most interval counting neurons. Relationship between pulse-number threshold before (baseline, x-axis) and after (y-axis) attenuating inhibition. Inhibition was attenuated either by focal iontophoresis of gabazine (gray circles) or intracellular loading of the cell with fluoride (black squares); pipette solution contained potassium fluoride. The dotted line represents no change in interval selectivity.

Discussion

Our results provide analyses of excitatory and inhibitory conductances in neurons that perform counting functions. We also combined, *in vivo*, whole-cell recording with focal pharmacological manipulation of inhibition to investigate its role in counting processes. We have shown that inhibition has onset and offset components and plays a prominent role in interval counting. PNTs, *i.e.*, the number of pulses, presented at the optimal rate, required for eliciting a threshold spike response, generally corresponded to the number of pulses required for full temporal separation of onset and offset phases of inhibitory conductances; the increase in net excitation during this “window” in the inhibition enabled suprathreshold depolarization. A single long interval, embedded in a sequence of optimal intervals, elicited offset inhibition and reset the interval-counting process. Similarly, behavioral experiments with gray treefrogs showed that a long interval reduced the attractiveness of calls to females (27). ICNs that had PNTs of 2 to 3 showed inhibition that was delayed in its onset, relative to that of excitation. Pharmacological results reinforced the conclusion that inhibition plays an important role in generating interval counting; attenuating inhibition reduced the PNTs of ICNs, and in several cases resulted in responses to single pulses, *i.e.*, abolished their interval-counting properties. We also found that ~31% of the ICNs for which conductance analyses were made showed little, if any, apparent inhibition. The interval-counting properties of these neurons were evident in the progression of mean excitation with pulse number. Like most ICNs that showed strong inhibition, single pulses elicited little, if any, excitation, which increased nonlinearly with increasing pulse number. Iontophoresis of gabazine, a GABA_A-receptor antagonist, attenuated inhibition as expected, but stimulus-driven increases in excitatory conductances were augmented as well—even in cases that appeared to have little inhibition. These increases in excitation strength could result from indirect effects of gabazine blocking inhibition on neighboring neurons that might provide excitatory input to the recorded cell. Alternatively, inhibitory inputs might shunt excitatory current from reaching the soma (26, 28); attenuating inhibition could decrease this shunting and increase excitatory

current that reaches the soma. To distinguish between these possibilities, we loaded neurons with fluoride to attenuate inhibition solely to the recorded neuron. As in a previous study (26) we found that excitatory conductances were also elevated after fluoride loading, suggesting that some shunting inhibition was present in these ICNs. Because this shunting was greatest when excitation and inhibition overlapped temporally, *e.g.*, for stimuli with subthreshold pulse numbers, excitation to these cells appeared more selective than was the case. Despite these increases in excitation, in most cases responses to 1- and 2-pulse stimuli, while elevated, remained subthreshold. Shunting effects of inhibition could also account for the decreases in mean Δg_e that occurred as the duration of a middle interval was increased, thereby recruiting additional inhibition.

Our results best support the Naud *et al.* “dis-inhibition” model of interval counting, which incorporates onset-type inhibition that depresses and offset inhibition (23). In this model, ICNs receive inhibitory inputs from neurons that are selective for long intervals, *i.e.*, slow pulse rates. These long-interval neurons (LINs, Fig. 1*F*) spike to individual pulses, thereby providing inhibition at each pulse to the ICNs. For a sequence of pulses presented at fast pulse rates, however, the model proposes that spike responses of LINs quickly decrease due to delayed inhibition to these cells, releasing the ICN from inhibition. Tonic excitation can then depolarize the ICN to threshold. At the end of the stimulus, postinhibitory rebound excitation in the LINs results in a strong offset-type inhibition to the ICN, which contributes to the resetting of the interval-counting process. This model differs substantially from that proposed earlier (13) in which inhibition was postulated to be tonic. Rate-dependent augmentation of excitation was postulated to shift the balance in its favor as pulses were repeated at optimal intervals; a long interval was presumed to reset the strength of the excitation to its low, baseline level. While our present results generally support the disinhibition model, they also indicate that some refinements may be needed. First, LINs showing postinhibitory rebound excitation have not been recorded thus far. Several lines of evidence suggest that onset and offset phases of inhibition may have different sources. One ICN was recorded that had a PNTs of 2 to 3 and showed only offset inhibition (Fig. 3*A*). The offset inhibition may, therefore, not result from postinhibitory rebound in the neurons that cause the inhibition at stimulus onset. Second, conductance analyses suggest that even single pulses elicit both onset and delayed, offset inhibition. Alternatively, onset and offset phases of inhibition may be mediated by conventional LINs (26) and neurons that show short-pass duration selectivity (25, 29), respectively. Third, many ICNs with high PNTs showed nonlinear increases in excitatory conductance following several pulses. Decreasing excitation strength increased PNTs, consistent with models of interval selectivity in which changes in the relative strengths of excitation and inhibition can alter interval tuning (30, 31). ICNs with high PNTs showed positive inflections in Δg_e for near-threshold numbers of pulses. Several origins of these inflections are possible. Excitation could gain strength as shunting inhibition (see above) decreases with successive pulses. The increase in Δg_e for subthreshold numbers of pulses following attenuation of inhibition (particularly for KF experiments) supports this mechanism; however, the nonlinearity and interval counting were not eliminated. Another, not mutually exclusive, possibility is that ICNs may receive inputs from cells that already show interval-counting properties, *i.e.*, hierarchical processing, as is seen in the model of Zemlianova *et al.* (Fig. 2*A*). Fourth, enhancement of presynaptic release could contribute to augmented excitation with successive pulses and, therefore, selectivity for high numbers of pulses. Neurons that respond after 2 sound pulses with specific timing have been recorded in

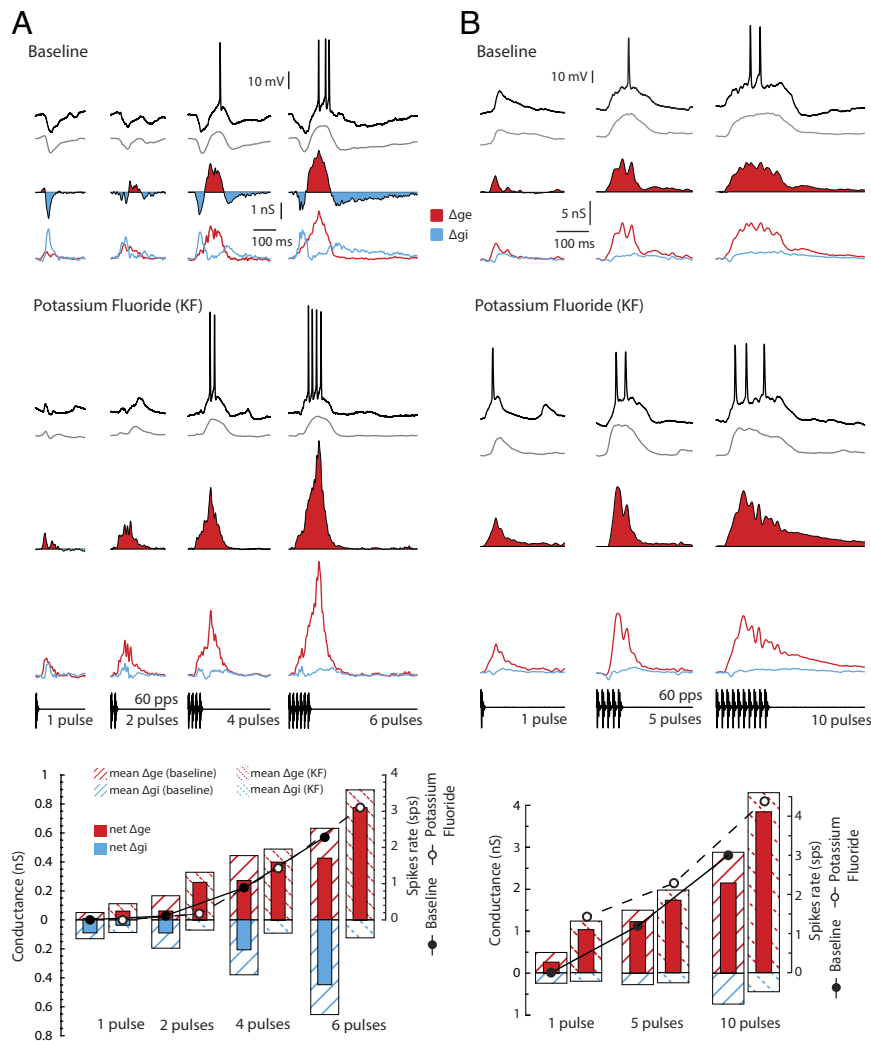


Fig. 9. Attenuating inhibition with KF decreases pulse-number threshold and increases excitatory conductances. Whole-cell membrane potential recordings, before (*Upper*) and after (*Lower*) loading with KF, of responses of two ICNs to stimuli that varied in pulse number; these interval-counting neurons showed prominent (*A*) or small (*B*) increases in Δg_i (inhibitory conductance, blue) above baseline. As in previous figures, estimates of changes in excitatory conductances (Δg_e , red) and inhibitory (Δg_i , blue) and their difference over time (area plots) are also shown. Mean and net conductances are displayed as striped and filled, respectively, bars in histograms; 45°- and -45°-striped bars represent baseline and KF conditions, respectively. Spikes per stimulus repetition are shown as solid or dotted lines for baseline and KF conditions, respectively. Resting potentials = -45 mV (*A*) and -75 mV (*B*); BEF = 340 Hz (*A*) and 240 Hz (*B*); stimulus amplitudes = 68 dB SPL (*A*) and 70 dB SPL (*B*). Pulse-number thresholds decreased from 4 to 3 pulses (*A*) and ~7 pulses to 1 pulse (*B*) before and after KF, respectively.

crickets (32); however, the mechanism that appears to underlie this interval “counting” and selectivity differs from that of ICNs. A first pulse elicits subthreshold excitation and strong inhibition; for an optimal interpulse interval, rebound depolarization then summates with excitation from a second pulse and elicits spiking. A similar mechanism could also underlie the interval selectivity of “delay-tuned” neurons in echolocating bats (33–35).

Numerical processes encompass a wide spectrum, ranging from learned, label-based counting to innate numerosity. The latter comprises abilities to identify the approximate number of like elements in a scene or that occur over time and is limited in its scope. In acoustic communication or music, it is most relevant to identify the number of sound elements that occur with specific timing. This temporal information can be represented in the distribution of activity in an array of ICNs. The subset of neurons in the array that are active reflects the number of sequential pulses that occurred with intervals that match values typical of specific communication signals; these cells can, therefore, constitute both sensory temporal filters and numerical processors. This combined function is to be expected given the biologically important roles of these neurons in call recognition. Neurons with low PNTs can

show strong interval selectivity, raising the question of why ICNs that require greater numbers of pulses exist. These cells may underlie the preferences of many anurans for longer calls (more pulses). Pulse number can also be a critical temporal feature that frogs use to discriminate between calls of males from different conspecific populations, e.g., in chorus frogs populations that are undergoing speciation (36). It is also important to note that male frogs can match the number of brief calls in a sequence (analogous to notes in a “phrase” of birdsong) emitted by a neighboring male (37–41); once matched, the other male generally adds an additional “pulse” to its next sequence, i.e., “one-ups” its competitor (15). This call number matching extends to as many as 7 to 8 calls in a sequence and demonstrates the numerical abilities of anurans. It remains to be seen whether ICNs exist that integrate over these longer intervals (~100 to 200 ms) (15).

The ability to accurately count intervals in a series of regularly spaced events is crucial for estimating elapsed time. For auditory neurons, this temporal information is present in the acoustic stimuli and coded in the timing of spikes in auditory-nerve fibers. Our results show that ICNs are selective to elapsed time, i.e., number of interpulse onset intervals. Specifically, the onset and offset

phases of inhibition approximately track the duration of the pulse train; the window in inhibition is accompanied by interval-count dependent ramping up of excitation that depolarizes the neuron to threshold. Furthermore, these ICNs exhibit a broad spectrum of pulse number thresholds, enabling them to measure elapsed time ranging from several milliseconds to at least 1 s.

More generally, interval-specific counting processes are potentially of great significance in enabling central nervous systems to decode information that is encoded in the number of spikes in bursts. Properties such as stimulus identity, salient information associated with location of an animal in its environment, and memories have been theorized to be encoded in bursts of spikes that have specific spike number and timing (19–21). Thus, interval counting neurons could operate generally to decode this information and represent it in “place” codes (22). In addition, counting intervals is a mechanism for estimating elapsed time and, therefore, time perception. The events that are counted can be external stimuli that occur at regular intervals and are coded in the timing of spikes, or internally generated discharges from a pacemaker (22). The general utility of ICNs decoding and/or time perception depends on how specialized the mechanisms are that underlie interval counting processes. Our results indicate that interval counting and selectivity results from integration of excitation and inhibition that has onset and offset components; these parameters are governed by time constants that dictate the interval dimensions over which the counting occurs. The mechanisms that underlie interval counting in anurans bear similarity to those that mediate short-interval selectivity in midbrain neurons in mormyrid electric fish (42). While not ICNs per se, these electrosensory neurons receive inhibition that depresses quickly at fast pulse rates and excitation that, in some cases, temporally summates. Similarly, hippocampal neurons show a rate-dependent shift in the balance of excitation and inhibition, with inhibition depressing at fast stimulation rates (43). In both systems, neurons could, therefore, perform counting functions. Thus, interval counting appears to utilize general properties of central nervous systems, which could be implemented across neural structures and brains to underlie numerosity, decode information coded/encoded in bursts of spikes and to estimate elapsed time.

Methods

Experimental Model and Subject Details. Wild-caught male and female northern leopard frogs (*Rana pipiens*) were group-housed at the University of Utah in a 3' × 2' × 1' plastic container with 1" of water at the bottom, situated in a room with a 12:12 h light/dark cycle. Frogs were fed live crickets twice a week. All care adhered to protocols approved by The University of Utah Animal Welfare Committee and followed NIH guidelines.

Method Details.

Surgical Preparation. Frogs were anesthetized by immersion in 3% urethane or 0.1% MS-222 and by topical application of 2% lidocaine hydrochloride to the skin of the dorsal surface of the head, where a small craniotomy was performed to expose the optic tectum. After a recovery period, frogs were immobilized by intramuscular injection of pancuronium bromide (4 µg/g) for electrophysiological recordings. Whole-cell patch recordings were made from neurons in the IC_{ant} in vivo, according to methods described previously (13, 44). Recordings were made in an audiometric chamber that was maintained at 18 to 20 °C. All procedures were conducted in compliance with the Society for Neuroscience's Policy on the Use of Animals in Neuroscience Research and the NIH guidelines and were approved by The University of Utah's Institutional Animal Care and Use Committee.

Electrode Construction. Patch pipettes were constructed from high-borate borosilicate capillary glass [Schott #8250, A-M Systems #5960; 1 mm outer diameter (OD), 0.58 mm inner diameter (ID)] using a Flaming/Brown type

puller (Sutter Instruments, model P-97). These pipettes had outside tip diameters of approximately 1.1 to 1.3 µm. Electrode tips were back-filled with a solution (pH = 7.4) consisting of (values in mM) 100 potassium gluconate, 2 KCl, 1 MgCl₂, 5 EGTA, 10 HEPES, 20 KOH, and 20 biocytin. Biocytin was replaced by mannitol (20 mM) in the solution used to fill pipette shanks. These pipettes had resistances between 8 and 20 MΩ. To block chloride channels, K⁺ gluconate and KCl were replaced with potassium fluoride (KF). Extracellular recording pipettes were manufactured from the same glass used for making patch pipettes, but had tip diameters of 2 to 3 µm and were filled with 2 M NaCl; resistances varied between 0.7 and 1.0 MΩ.

Whole-Cell Recording Procedure. “Whole-cell” recordings were made with patch-type pipettes, as described previously (13, 44). Briefly, recording pipettes were advanced into the brain using an “inch-worm” microdrive (Burleigh Corp., model 6,000 Controller) or a 3-axis microdrive (Scientifica PLC, model IVM-3000) while applying positive pressure to the pipette fluid. After reaching the location for whole-cell recording, the pipette was advanced in 1.5 µm increments while maintaining positive pressure and passing -0.1 nA square-wave pulses (500 ms) to monitor resistance; cell contact was indicated by a small increase (10%) in the voltage change. Negative pressure was then applied to the pipette to increase the seal resistance to giga-ohm levels. Subsequent to seal formation, negative current (~-0.5 nA) was applied to rupture the patch and attain a whole-cell recording. Seal resistances were typically greater than 1.5 GΩ. Reported resting potentials are uncorrected for liquid junction potential. Recordings were made in “current-clamp” vs. voltage-clamp mode. Computer simulations (45, 46) and direct experimental measurements (47) have demonstrated that it is not possible to accurately control the voltage in dendritic compartments using the somatic voltage-clamp method. Stimulus-driven changes in excitatory and inhibitory conductances could be estimated (described below) using recordings at several levels of constant, negative current injection (48). While both methods can estimate synaptic conductances only as they affect changes in the somatic membrane potential, the current-clamp method has several advantages: Compensations for voltage drops across series resistances (electrode and patch) at the time of the recording are not required and injection of positive current, which is used in voltage-clamp experiments and activates voltage-dependent conductances, is avoided.

Pharmacological Procedure. We delivered drugs iontophoretically, using 3- to 5-barrel micropipettes, as described previously (26). Individual barrels were filled with L-glutamate (100 mM, pH = 8.0), NaCl (150 mM) for current balance, gabazine (3 mM in 150 mM NaCl, pH = 4.0) or bicuculline methiodide (20 mM in 150 mM NaCl, pH = 3.0) to block GABA_A receptors, 5 mM NBQX (1,2,3,4-tetrahydro-6-nitro-2,3-dioxo-benzo [f]quinoxaline-7-sulfonamide) (pH 9.0 in 150 mM NaCl) to block AMPA/kainate. Each barrel of the assembly was connected via an Ag/AgCl wire to a constant-current iontophoresis device (Dagan Corp., model 6400). Approximately 50 to 100 nA constant current was used to iontophoretically deliver pharmacological compounds (negative for glutamate, NBQX and CPP, positive for gabazine). We iontophored glutamate to activate recorded cells and to assess whether the multibarrel pipette was sufficiently close for conducting pharmacological manipulations (24). To minimize leakage of agents, retention currents of approximately 5 nA (opposite the polarity used to deliver the agents) were applied to barrels that contained drugs. Multibarrel pipettes were advanced into the brain using a single-axis hydraulic manipulator (Siskiyou Corporation, model MX610). For experiments involving intracellular fluoride, potassium gluconate in the intracellular solution was replaced by potassium fluoride. Baseline recordings were made as soon as cell access was achieved; current-clamp levels of 0 to -0.06 nA were used. Attenuation of inhibition from injection of KF was marked by an increase in spike rate or strength of depolarizations. These effects were clearly observed on average approximately 3 mins after baseline recordings were completed and KF was delivered (~-0.1 nA); recordings with KF-attenuated inhibition were, on an average, approximately 13 mins after achieving access to the cell.

Stimulus Generation and Delivery. Acoustic stimuli were generated using an auditory stimulus generator (Tucker Davis Technologies, systems II & III) and custom software developed in Matlab environment (MathWorks, Inc.). Search stimulus carrier frequencies were systematically varied from 150 to 1,600 Hz with modulation frequencies (in the case of sinusoidal amplitude modulation, SAM) ranging from 10 Hz to 100 Hz. To test for interval selectivity, pulse duration and number were held constant and only pulse rate was varied, usually from 5 to 80 pulses/s. Stimuli were presented free-field and contralateral to the recording site in an audiometric room (17).

Data Acquisition. Recordings were acquired and digitized at 10 kHz using a data acquisition interface (Cambridge Electronic Design, Model: Power 1401), then stored, and analyzed using Spike2 software, also from the same supplier.

Conductance Reconstruction. Estimates of excitatory and inhibitory conductances were determined according to methods described previously (26). Spike threshold E_s was approximated across responses for repeated stimulus presentations. The subthreshold ($V < E_s$) membrane potential changes consisted of two parts: 1) linear changes in synaptic currents and membrane potential and 2) nonlinear changes due to voltage-dependent activation of synaptic and/or intrinsic currents. We define the boundary between linear and nonlinear variations (near-threshold) as the activation potential (E_{act}). The subthreshold linear changes in $V (\leq E_{act})$ can be accurately modeled using Eq. 1; however, this is not the case for nonlinear subthreshold variations (49) (Priebe and Ferster, 2008).

$$C \frac{dV(t)}{dt} = I_{inj}(t) - \Delta g_e(t)(V(t) - E_e) - \Delta g_i(t)(V(t) - E_i) - g_{leak}(V(t) - E_r) \quad [1]$$

where C is the cell capacitance, E_i and E_e are the reversal potentials of the inhibitory and excitatory conductances, V is the membrane potential (expressed as a function of time), $g_{leak} = 1/R_{input}$ (represents the sum of conductances responsible for holding the cell at its resting potential, E_r), and I_{inj} is the current injected into the cell through the patch pipette (electrode). The input resistance (R_{input}) and time constant (τ) of the cell were estimated (double exponential curve fit, in Spike-2) from brief negative current pulses delivered to the neuron; the voltage drop across the electrode and access resistances, which had a faster time course, was subtracted from the total voltage change produced by these current injection steps; $R_{input} = V/I_{inj}$. In addition to measuring this voltage drop and subtracting it from the apparent membrane potential, we used a spike-threshold based method of determining V (50). This approach is based on the assumption that spike threshold for a particular neuron should, on average, be constant across current clamp conditions. Thus, to determine the actual membrane potential following current injection, the spike threshold drop was subtracted from the apparent membrane potential change. The mean input resistance of neurons in this study was approximately 420 M Ω . The capacitance of each neuron was calculated as $C = \tau/R_{input}$. The inhibitory reversal potential for each cell was estimated to be the V at which IPSPs reversed from hyperpolarizations to depolarizations; in some cases, carrier frequencies that elicited primarily inhibition were used for determining these reversal potentials. The excitatory reversal potential was based on measurements where EPSPs were reversed from depolarizations to hyperpolarizations. While the relative magnitudes of changes in excitation (Δg_e) and inhibition (Δg_i) changed slightly for different values of these reversal potentials, the time courses of these conductances were not affected. The computed Δg_e and Δg_i values represent estimates of stimulus-related changes in conductances relative to prestimulus baseline levels; background (no stimulus present) excitatory and inhibitory conductances contributed to the "leak" conductance, g_{leak} . Recordings without current injection and at small levels of current clamp in some cases showed evidence of active membrane properties that amplified depolarizations. For these cases, we performed analyses in which a nonlinear term, based on the hybrid model suggested by Izhikevich (51), was added to the above Eq. 1.

$$C \frac{dV(t)}{dt} = \alpha (V(t) - E_t) (V(t) - E_r) + \beta (V(t) - E_r) + I_{inj}(t) - \Delta g_e(t) (V(t) - E_e) - \Delta g_i(t) (V(t) - E_i) - g_{leak} (V(t) - E_r) \quad [2]$$

where

$$\alpha = \frac{g_l}{2(E_{act} - E_r)} \quad [3]$$

$$\beta = \frac{g_l}{2(E_{act} - E_r)} (E_t - E_r) \quad [4]$$

Details of this method can be found in ref. 26.

1. B. Butterworth, C. Gallistel, G. Vallortigara Introduction: The origins of numerical abilities. 20160507 (The Royal Society, 2018).
2. A. Nieder, Evolution of cognitive and neural solutions enabling numerosity judgements: Lessons from primates and corvids. *Philos. Trans. R Soc. B Biol. Sci.* **373**, 20160514 (2018).
3. A. Nieder, Neuroethology of number sense across the animal kingdom. *J. Exp. Biol.* **224**, jeb218289 (2021).

We used a least-squares approach to estimate the changes in excitatory (Δg_e) and inhibitory (Δg_i) conductances of a neuron in response to stimuli. This minimization process involved overdetermining the system, i.e., using recordings at multiple levels of negative current clamp (injected current) to obtain more equations than the number of unknown parameters (in this case, Δg_e and Δg_i). We approximated Δg_e and Δg_i at each sample point in time (0.1 ms) as the values that provided the best fit, i.e., minimized the difference between measured and calculated changes in membrane potential, for the recordings across all current clamp levels (25).

Mean and Net Conductances. For comparing excitatory and inhibitory conductance amplitudes across pulse rates, mean values of responses of cells to each stimulus were computed over the time period of the conductances for the longest stimulus used in the analyses. To quantify Δg_e and Δg_i , we computed the mean of their time courses for the duration of response, i.e. sum of values at every time sample divided by the total number of samples. Net Δg_e is the mean of positive values and net Δg_i is the absolute mean of negative values of the difference ($\Delta g_e - \Delta g_i$) at each time point. Therefore, net Δg_e represents the resultant excitation that is not counteracted by inhibition and net Δg_i represents the resultant inhibition that is not counteracted by excitation.

The percentage drop in the means and net conductances across pulse number (ΔN) were calculated as:

$$\% \text{drop in } \Delta g \text{ across } \Delta N \text{ pulses} = \frac{\Delta g \text{ at } N \text{ pulses} - \Delta g \text{ at } (N - \Delta N) \text{ pulses}}{\Delta g \text{ at } N \text{ pulses}} * 100. \quad [5]$$

The normalized conductance means were computed as:

$$\text{normalized } \Delta g \text{ at } N \text{ pulses} = \frac{\Delta g \text{ at } N \text{ pulses}}{\Delta g \text{ at } PNT} \quad [6]$$

The mean/net Δg slope was calculated using the difference in Δg over the change in pulse number (ΔN).

$$\text{slope of } \Delta g = \frac{\Delta g \text{ at } N \text{ pulses} - \Delta g \text{ at } (N - \Delta N) \text{ pulses}}{\Delta N \text{ pulses}} \quad [7]$$

where $N >= 1$ pulse and $N <= PNT$.

For most cases with pulse increments greater than one, the pulse number for the peak mean Δg slope was determined through interpolation.

Regression. Linear regression was executed in Matlab, followed by the Lilliefors test for assessing the normality of the regression residuals. The hypothesis that the residuals were derived from a normal distribution could not be rejected for any of the regressions presented in this paper. Prior to regression, data pertaining to pulse number thresholds were transformed logarithmically. To examine multicollinearity, the Variance Inflation Factor (VIF) was calculated for each variable, with all VIFs found to be less than 3, indicating no significant multicollinearity.

Data, Materials, and Software Availability. The datasets generated and/or analyzed during the current study and the data & code required for analysis were deposited in the UHive repository: <http://doi.org/10.7278/55d-0nnd-9r1n> (52). All other study post-analysis data are included in the article and/or [Supporting Information](#).

ACKNOWLEDGMENTS. This work was supported by NIDCD grant R01 DC017644.

Author affiliations: ^aSchool of Biological Sciences, University of Utah, Salt Lake City, UT 84112; ^bDepartment of Psychology, University of California, Los Angeles, CA 90095; ^cDepartment of Biology, University of Mississippi, Oxford, MS 38677; ^dDepartment of Psychological and Brain Sciences, Dartmouth College, Hanover, NH 03755; and ^eDepartment of Neurobiology, School of Medicine, University of Utah, Salt Lake City, UT 84112

Author contributions: R.K.A., G.J.R., and C.J.L. designed research; R.K.A., G.J.R., J.M., A.M., C.J.L., J.A.G., and G.A.V.-O. performed research; R.K.A. and G.J.R. contributed new reagents/analytic tools; R.K.A., G.J.R., J.M., and A.M. analyzed data; and R.K.A., G.J.R., J.M., and C.J.L. wrote the paper.

4. P. Skorupski, H. MaBouDi, H. S. Galpayage Dona, L. Chittka, Counting insects. *Philos. Trans. R Soc. B Biol. Sci.* **373**, 20160513 (2018).
5. C. R. Gallistel, Finding numbers in the brain. *Philos. Trans. R Soc. London B Biol. Sci.* **373**, 20170119 (2018).
6. S. Dasgupta, D. Hattori, S. Navlakha, A neural theory for counting memories. *Nat. Commun.* **13**, 5961 (2022).

7. E. F. Kutter, J. Bostroem, C. E. Elger, F. Mormann, A. Nieder, Single neurons in the human brain encode numbers. *Neuron* **100**, 753–761.e4 (2018).
8. A. Nieder, I. Diester, O. Tudusciuc, Temporal and spatial enumeration processes in the primate parietal cortex. *Science* **313**, 1431–1435 (2006).
9. A. Nieder, E. K. Miller, A parieto-frontal network for visual numerical information in the monkey. *Proc. Natl. Acad. Sci. U.S.A.* **101**, 7457–7462 (2004).
10. H. M. Ditz, A. Nieder, Neurons selective to the number of visual items in the corvid songbird endbrain. *Proc. Natl. Acad. Sci. U.S.A.* **112**, 7827–7832 (2015).
11. L. Wagener, M. Loconsole, H. M. Ditz, A. Nieder Neurons in the endbrain of numerically naive crows spontaneously encode visual numerosity. *Curr. Biol.* **28**, 1090–1094.e4 (2018).
12. C. J. Edwards, T. B. Alder, G. J. Rose, Auditory midbrain neurons that count. *Nat. Neurosci.* **5**, 934–936 (2002).
13. C. J. Edwards, C. J. Leary, G. J. Rose, Counting on inhibition and rate-dependent excitation in the auditory system. *J. Neurosci.* **27**, 13384–13392 (2007).
14. G. J. Rose, Time computations in anuran auditory systems. *Front. Physiol.* **5**, 206 (2014).
15. G. J. Rose, The numerical abilities of anurans and their neural correlates: Insights from neuroethological studies of acoustic communication. *Philos. Trans. R. Soc. B Biol. Sci.* **373**, 20160512 (2018).
16. T. B. Alder, G. J. Rose, Long-term temporal integration in the anuran auditory system. *Nat. Neurosci.* **1**, 519–523 (1998).
17. T. B. Alder, G. J. Rose, Integration and recovery processes contribute to the temporal selectivity of neurons in the midbrain of the northern leopard frog, *Rana pipiens*. *J. Comp. Physiol. A* **186**, 923–937 (2000).
18. J. S. Mecham, Vocalizations of the leopard frog, *Rana pipiens*, and three related Mexican species. *Copeia* **1971**, 505–516 (1971).
19. R. Naud, H. Sprekeler, Sparse bursts optimize information transmission in a multiplexed neural code. *Proc. Natl. Acad. Sci. U.S.A.* **115**, E6329–E6338 (2018).
20. A. Payeur, J. Guerguiev, F. Zenke, B. A. Richards, R. Naud, Burst-dependent synaptic plasticity can coordinate learning in hierarchical circuits. *Nat. Neurosci.* **24**, 1010–1019 (2021).
21. F. Zeldenrust, W. J. Wadman, B. Englitz, Neural coding with bursts—current state and future perspectives. *Front. Comput. Neurosci.* **12**, 48 (2018).
22. K. Zemlianova, A. Bose, J. Rinzel, A biophysical counting mechanism for keeping time. *Biol. Cybern.* **116**, 1–14 (2022).
23. R. Naud, D. Houtman, G. J. Rose, A. Longtin, Counting on dis-inhibition: A circuit motif for interval counting and selectivity in the anuran auditory system. *J. Neurophysiol. (Bethesda)* **114**, 2804–2815 (2015).
24. G. J. Rose *et al.*, Combining pharmacology and whole-cell patch recording from CNS neurons, in vivo. *J. Neurosci. Methods* **213**, 99–104 (2013).
25. R. K. Alluri *et al.*, Phasic, suprathreshold excitation and sustained inhibition underlie neuronal selectivity for short-duration sounds. *Proc. Natl. Acad. Sci. U.S.A.* **113**, E1927–E1935 (2016).
26. R. K. Alluri *et al.*, How auditory selectivity for sound timing arises: The diverse roles of GABAergic inhibition in shaping the excitation to interval-selective midbrain neurons. *Progress Neurobiol.* **199**, 101962 (2021).
27. J. J. Schwartz, K. Huth, R. Hunce, B. Lentine, Effect of anomalous pulse timing on call discrimination by females of the gray treefrog (*Hyla versicolor*): Behavioral correlates of neurobiology. *J. Exp. Biol.* **213**, 2066–2072 (2010).
28. A. Gidon, I. Segev, Principles governing the operation of synaptic inhibition in dendrites. *Neuron* **75**, 330–341 (2012).
29. C. J. Leary, C. J. Edwards, G. J. Rose, Midbrain auditory neurons integrate excitation and inhibition to generate duration selectivity: An in vivo whole-cell patch study in anurans. *J. Neurosci.* **28**, 5481–5493 (2008).
30. D. V. Buonomano, Decoding temporal information: A model based on short-term synaptic plasticity. *J. Neurosci.* **20**, 1129–1141 (2000).
31. D. V. Buonomano, Neural dynamics based timing in the subsecond to seconds range. *Adv. Exp. Med. Biol.* **829**, 101–117 (2014).
32. S. Schöneich, K. Kostarakos, B. Hedwig, An auditory feature detection circuit for sound pattern recognition. *Sci. Adv.* **1**, e1500325 (2015).
33. W. E. O'Neill, N. Suga, Target range-sensitive neurons in the auditory cortex of the mustache bat. *Science* **203**, 69–73 (1979).
34. C. V. Portfors, J. J. Wenstrup, Delay-tuned neurons in the inferior colliculus of the mustached bat: Implications for analyses of target distance. *J. Neurophysiol.* **82**, 1326–1338 (1999).
35. N. Suga, Neural processing of auditory signals in the time domain: Delay-tuned coincidence detectors in the mustached bat. *Hearing Res.* **324**, 19–36 (2015).
36. E. M. Lemmon, Diversification of conspecific signals in sympatry: Geographic overlap drives multidimensional reproductive character displacement in frogs. *Evol.: Int. J. Organic* **63**, 1155–1170 (2009).
37. A. Arak, Vocal interactions, call matching and territoriality in a Sri Lankan treefrog, *Phyllautus leucorhinus* (Rhacophoridae). *Animal Behav.* **31**, 292–302 (1983).
38. H. C. Gerhardt, J. D. Roberts, M. A. Bee, J. J. Schwartz, Call matching in the quacking frog (*Crinia georgiana*). *Behav. Ecol. Sociobiol.* **48**, 243–251 (2000).
39. A. S. Rand, M. J. Ryan, The adaptive significance of a complex vocal repertoire in a neotropical frog. *Ethology* **57**, 209–214 (1981).
40. M. J. Ryan, Frequency modulated calls and species recognition in a neotropical frog. *J. Comp. Physiol. A: Neuroethol., Sensory, Neural, Behav. Physiol.* **150**, 217–221 (1983).
41. J. J. Schwartz, Male calling behavior and female choice in the neotropical treefrog *Hyla microcephala*. *Ethology* **73**, 116–127 (1986).
42. C. A. Baker, B. A. Carlson, Short-term depression, temporal summation, and onset inhibition shape interval tuning in midbrain neurons. *J. Neurosci.* **34**, 14272–14287 (2014).
43. M. Mori, M. H. Abegg, B. H. Gähwiler, U. Gerber, A frequency-dependent switch from inhibition to excitation in a hippocampal unitary circuit. *Nature* **431**, 453–456 (2004).
44. G. J. Rose, E. S. Fortune, New techniques for making whole-cell recordings from CNS neurons in vivo. *Neurosci. Res.* **26**, 89–94 (1996).
45. D. Johnston, T. H. Brown, Interpretation of voltage-clamp measurements in hippocampal neurons. *J. Neurophysiol.* **50**, 464–486 (1983).
46. N. Spruston, D. B. Jaffe, S. H. Williams, D. Johnston, Voltage- and space-clamp errors associated with the measurement of electrotonically remote synaptic events. *J. Neurophysiol.* **70**, 781–802 (1993).
47. S. R. Williams, S. J. Mitchell, Direct measurement of somatic voltage clamp errors in central neurons. *Nat. Neurosci.* **11**, 790–798 (2008).
48. N. J. Priebe, D. Ferster, Direction selectivity of excitation and inhibition in simple cells of the cat primary visual cortex. *Neuron* **45**, 133–145 (2005).
49. N. J. Priebe, D. Ferster, Inhibition, spike threshold, and stimulus selectivity in primary visual cortex. *Neuron* **57**, 482–497 (2008).
50. J. S. Anderson, I. Lampl, D. C. Gillespie, D. Ferster, Membrane potential and conductance changes underlying length tuning of cells in cat primary visual cortex. *J. Neurosci.* **21**, 2104–2112 (2001).
51. E. M. Izhikevich, Hybrid spiking models. *Philos. Trans. R. Soc. London A: Math., Phys. Eng. Sci.* **368**, 5061–5070 (2010).
52. R. K. Alluri *et al.*, Whole-cell, in vivo, recording data for interval counting neurons in the inferior colliculus of *R. pipiens*. UHive. <http://doi.org/10.7278/ISSd-0nnd-9r1n>. Deposited 31 July 2024.